Three-Stage Distribution Feeder Control Considering Four-Quadrant EV Chargers

Mauricio Restrepo, *Student Member, IEEE*, Claudio A. Cañizares, *Fellow, IEEE*, Mehrdad Kazerani, *Senior Member, IEEE*

***Abstract*—With the increased penetration of electric vehicle (EV) chargers in distribution systems, there is a need to understand and minimize their impact on medium-voltage (MV) and low-voltage (LV) networks. Thus, this paper proposes a three-stage algorithm to coordinate the operation of four-quadrant EV chargers with other volt/var control devices in MV and LV distribution feeders. The First Stage operates on a day-ahead basis and defines the load tap changer (LTC) and capacitor schedules while minimizing the peak load associated with EVs in the distribution system. The second and third stages update their operation every five minutes, to fairly allocate the aggregated and individual EV loads in the MV an LV feeders, respectively, while minimizing active power losses and voltage deviations. The proposed technique is applied to CIGRE's North-American MV and LV benchmark systems to demonstrate its ability to properly allocate EV loads, and improve distribution system performance in terms of losses and voltage deviations.**

***Index Terms*—Four-quadrant electric vehicle charger, charging control, medium-voltage networks, low-voltage networks, electric vehicle, vehicle-to-grid, distribution system management.**

NOMENCLATURE

Indices

$agev$	Aggregated EV index
bl	Base load
ev	EV index
fin	Final
i	Tap index
ini	Initial
j	Switched capacitor index
k	MV bus number
L_m, L_l	MV and LV load indexes
l_m, l_l	MV and LV line indexes
n_m, n_l	MV and LV node indexes
$nev_{n_m,t}$	Number of EVs at node n_m at time t
p	Phase index
r	Line's receiving end
s	Line's sending end
t	Time index

Parameters

α, β	Second Stage objective function weight factors
γ	Heuristic method scaling factor
$\overline{cap}$	Maximum switching capacitor position
$\overline{E}$	Maximum energy capacity [kWh]
$\overline{I}$	Maximum line current [p.u.]
$\overline{S}$	Maximum apparent power [kVA]
$\overline{tap}, \underline{tap}$	Maximum and minimum tap positions
$\overline{V}, \underline{V}$	Maximum and minimum voltage limits [p.u.]
τ_1, τ_2	Time steps for stages 1 and 2
θ	Line admittance angle [rad]
$ABCD$	ABCD parameter matrices
Bc	EV battery capacity [kWh]
Cr	EV charger rating [kVA]
LN	Number of load nodes in the MV system
Mop	Maximum number of operations per hour
N	Number of nodes in the MV system
P_{max}	Maximum allowable peak demand
T	Maximum time
Y	Line admittance magnitude [S]
Z	Impedance [Ω]

Variables

δ	Voltage angle [rad]
cap	Switched capacitor position
E	Energy [kWh]
I	RMS current [p.u.]
P	Active Power [kW]
Q	Reactive Power [kVAR]
S	Apparent Power [kVA]
SoC	State of Charge
tap	Tap position
V	RMS voltage [p.u.]
VD	MV voltage deviation index [p.u.]

This work was supported by an NSERC collaborative research and development grant (CRD) and Ontario research fund (ORF) grant, in collaboration with Hydro One Networks Inc. and IBM.

M. Restrepo, C. Cañizares, and M. Kazerani are with the Department of Electrical and Computer Engineering, University of Waterloo, Waterloo, ON N2L 3G1, Canada (emails: mrestrep@uwaterloo.ca; ccanizares@uwaterloo.ca; mkazerani@uwaterloo.ca)

I. INTRODUCTION

NOWADAYS, the share of full and plug-in hybrid electric vehicles (EVs) in the global passenger car fleet is marginal; however, in the coming years, this share is expected to increase significantly thanks to a larger number of EV alternatives and lower prices. Through the end of 2015, around 1.26 million EVs were in operation worldwide, representing only 0.1% of overall passenger car fleet; however, in countries such as Netherlands, Norway, Sweden and US, EV sales have reached over 1% of total passenger car sales [1].

Rising penetration of EVs will create new challenges for the operation of power systems, since more electricity needs to be produced and delivered to these loads using the existing infrastructure. Thus, operating problems such as thermal overloads

and out-of-range voltages will become common, requiring expensive upgrades to distribution and transmission systems [2]. However, these investments can be deferred and/or minimized using smart charging technologies, which control the time and level of charging to flatten the load curve and reduce the charging costs by shifting the charging loads to low-demand, low-electricity price periods. The implementation of this concept has been proposed extensively in the literature using different control architectures, objective functions, communication and computation requirements, and market integration models [3]. In fact, some utilities and companies are actively implementing smart charging mechanisms and systems [4].

The majority of works in smart charging have considered unidirectional chargers, and some works have contemplated bidirectional chargers to charge and discharge the EV batteries in vehicle-to-grid (V2G) schemes for providing ancillary services and supporting the operation of renewable energy sources [5]. However, several works have looked at four-quadrant EV chargers and the possibility of exchanging reactive power with the grid. In [6], the potential of reactive power support operation of various single-phase EV charger topologies is explored, concluding that bidirectional chargers can provide reactive power support independently of battery charging within the volt-ampere capability of the charger; however, the dc link capacitor size needs to be enlarged in this case since the dc link voltage ripple increases when the charger provides reactive power support. Moreover, the ability of providing reactive power with bidirectional EV chargers has been demonstrated practically with prototypes in [7] and [8], for single-phase, Level 1 chargers; in [9], for a single-phase, Level 2 charger; and in [10], for a three-phase, Level 3 charger.

Volt/var regulation function is typically performed in distribution systems with LTCs, step voltage regulators (SVRs) and capacitor banks. Recently, due to the penetration of distributed generators (DGs) with the possibility of regulating reactive power, new challenges have emerged in the conventional volt/var function, which have been addressed in several works (e.g., [11]–[14]). Particularly, the impact of wind resource uncertainty in DG reactive power availability is difficult to model in volt/var analyses, although some works have proposed approaches to overcome this problem [15], [16]. In the near future, the inclusion of EV chargers with reactive power control will modify the conventional volt/var control function, which should coordinate the aforementioned control devices, DGs, and EVs. Thus, in [17], a cooperative method to compensate for undervoltages based on local voltage measurements, EV chargers with reactive power injection capacity, and communication links is presented; however, the algorithm does not consider the coordination with other volt/var regulation devices, and does not prioritize the charging function over the reactive power provision. These drawbacks are also seen in [18], which proposes a two-stage optimization algorithm for controlling four-quadrant EV chargers to flatten the demand curve, reduce the system currents, and minimize losses, and in [19], which formulates a multi-objective optimization algorithm that minimizes parking and charging costs from the user perspective, and minimizes reactive power service costs provided by EVs from the utility point of view. The authors in [20] propose a receding horizon control framework for scheduling four-quadrant EV chargers considering technical constraints such as maximum DC current ripples in EV chargers and battery degradation costs; however, in this framework, neither the power system topology nor other volt/var control devices are considered. Reference [21] investigates a centralized volt/var optimization engine which considers LTCs, SVRs, capacitor banks, and four-quadrant EVs to minimize power losses and capacitor operation costs, accounting for distribution system topology and the operation constraints of the volt/var regulation devices; however, EVs are considered only to inject reactive power and are aggregated in different MV nodes, without calculating the individual EV charger set points. A real-time, three-stage scheme for voltage regulation in distribution feeders, which considers simultaneous operation of LTCs, solar photovoltaics (PVs), and EVs is reported in [22]. This scheme gives priority to EV charging and PV active power injection, and uses the remaining reactive power operation capacity of PV inverters and EVs to reduce the number of operations of LTCs; however, it does not calculate the individual set-points for EVs, and does not allocate the charging and generated power among PVs and EVs in a fair manner.

From the previous discussion regarding using four-quadrant EV chargers for the volt/var control, it can be concluded that it is still necessary to account for the uncertainty of EV owner's behavior in terms of energy consumption, connection and disconnection times, coordination of four-quadrant EV chargers with other equipment in the volt/var function, and calculation of individual set points for EVs in the LV network, where they are actually connected. Thus, this paper complements the two-stage scheme presented in [23] and [24], by introducing the modeling of four-quadrant EV chargers for providing reactive power services, and adding a Third Stage in which the individual set points of EVs are determined. Hence, the main objectives and contributions of the present paper are the following:

- Propose and validate a three-stage approach to minimize system losses and peak load, provide adequate volt/var support, and fairly allocate EV charging load, based on a four-quadrant EV smart charger, connected at the LV distribution system level.
- Consider the uncertainty of EV driving behavior to properly model the active and reactive power demand of four-quadrant EV smart chargers, and determine optimal day-ahead and appropriate transformer tap and capacitor schedules.
- Consider both MV and LV networks, in which EV chargers represent a significant load compared to other household loads, to generate practical smart charging control signals for individual EVs connected at the LV level.
- Test the proposed approach on realistic MV and LV North-American distribution networks, and compare it with an existing volt/var regulation strategy, demonstrating its benefits and practical feasibility.

The remaining of this paper is organized as follows: Section II briefly discusses the implications of four-quadrant EV chargers in the typical distribution feeders' volt/var function, and describes the proposed three-stage architecture for distribution feeder and EV charging control. Then, Section III introduces the mathematical model of each stage of the proposed architecture, and Section IV discusses the simulation results and analysis of the proposed control approach and an existing volt/var regulation strategy in a CIGRE's benchmark test system. Finally, Section V presents the main conclusions and contributions of this paper.

II. Background

A. Volt/var Control in Distribution Feeders

The control problem in distribution feeders has been treated traditionally as a volt/var problem. For this purpose, LTCs at the main substation, capacitors at the substation level, capacitors at the feeder level, and SVRs [11] are used. The objectives of typical volt/var control are to minimize voltage deviations, maintain a power factor near unity at all nodes along the feeder, minimize the power losses in the system, keep the loading of lines and transformers within limits, and minimize the total number of tap changing and switching operations.

Four-quadrant EV chargers that are able to exchange reactive power with the grid will modify the traditional way the volt/var control devices are operated. This may require communication links between the grid operator and the EV charger, but would imply a lower number of capacitor switching and tap changing operations, and better controlability of the feeder, since more reactive power sources will be distributed along the feeder. The proposed architecture for coordinating four-quadrant EV chargers with other devices that perform volt/var control function in distribution feeders is explained next.

B. Proposed Three-Stage Architecture

The three-stage control architecture proposed for coordination of the operation of four-quadrant EV chargers, LTCs, and switched capacitors is presented in Fig. 1. This scheme is based on the work reported in [23] and [24], which is enhanced here by adding the modeling of four-quadrant EV chargers, the objective functions related to reactive power operation, and the individual EV charger set-point modulation. The control architecture accounts for the uncertainty in EV operation, i.e., the energy consumed during a day, and the charger's connection and disconnection times, providing individual set-points for the EV chargers connected to the LV system. The First Stage of the proposed architecture consists of a stochastic day-ahead dispatch of taps and capacitors, considering the probabilistic modeling of EV operation in terms of battery state of charge (SoC), arrival time, and departure time, as explained in some detail in Section III-A. This information can be obtained from studies that track operational data of EVs, as is the case here. This stage considers only the MV feeder; thus, the LV loads and EVs are aggregated at the respective MV node. The inputs of this stage are the feeder's load and

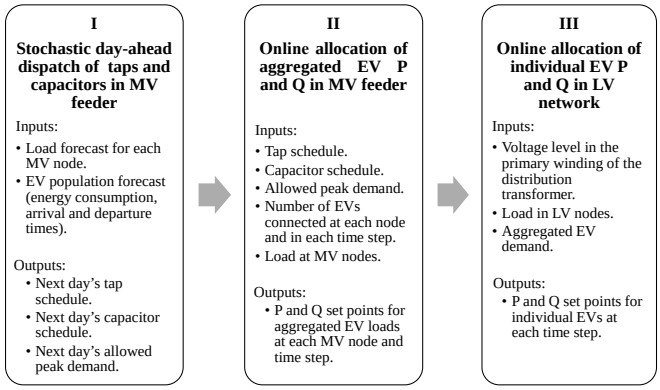

Fig. 1. Proposed three-stage architecture for controlling four-quadrant EV chargers in distribution feeders.

EV population forecasts and their probabilistic characteristics, and the outputs are the best estimate for capacitor switching schedule, transformer tap schedule, and allowed peak demand for the next day. The Second Stage allocates the EV aggregated load every 5 minutes, using the tap and capacitor settings, maximum allowable load, and the actual number of EVs connected at each node. Finally, the Third Stage receives the aggregated set-points from the Second Stage and allocates them individually to the EVs connected to the system, based on the conditions calculated on the Second Stage at the MV node, and the actual household demand.

The proposed control architecture has been designed to be implemented as a hierarchical distributed control. Stages 1 and 2 are conceived to be carried out by a central controller, and the third stage by distributed controllers located at the same levels as the distribution MV/LV transformers. Based on this, the interplay among the three stages will be hierarchical, with the distributed controllers following the signals calculated centrally, and communicating the results back to the central controller to guarantee coordination with the rest of the system.

III. Mathematical models

In this section, the mathematical models for each stage of the proposed control architecture are introduced and explained.

A. First Stage

This stage operates one day ahead of the actual implementation, with the objective of minimizing the peak load as follows:

$$\min P^{max} = \max_{t=1,..,T} \sum_{n_m=1}^{N} \left(P^{bl}_{n_m,t} + P^{agev}_{n_m,t} \right) \qquad (1)$$

assuming that only the EV load, represented in (1) as $P^{agev}_{n_m,t}$, can be controlled. The base load profile, represented in (1) as $P^{bl}_{n_m,t}$, is obtained from forecast information and is kept constant during the simulation; however, this is modeled as a constant impedance and hence presents deviations from the base value when the node voltages in the system are different from 1 p.u.

The constraints that accompany the objective function (1) are the following:

$$\sum_{t=1}^{T} P_{n_m,t}^{agev} \tau_1 \leq E_{agev_{n_m}} \ \forall n_m = 1, ..., LN \tag{2}$$

$$\overline{E_{agev_{n_m}}} = \sum_{ev=1}^{nev_{n_m}} Bc_{ev} \ \forall n_m = 1, ..., LN \tag{3}$$

$$\sum_{t=1}^{T} P_{n_m,t}^{agev} \tau_1 \geq (SoC_{agev_{n_m}}^{fin} - SoC_{agev_{n_m}}^{ini}) \overline{E_{agev_{n_m}}} \quad \forall n_m = 1, ..., LN \tag{4}$$

$$\overline{S_{n_m,t}^{agev}} = \sum_{ev=1}^{nev_{n_m},t} Cr_{ev} \ \forall n_m = 1, ..., LN, \forall t \tag{5}$$

$$0 \leq P_{n_m,t}^{agev} \leq \overline{S_{n_m,t}^{agev}} \ \forall n_m = 1, ..., LN, \forall t \tag{6}$$

$$-\overline{S_{n_m,t}^{agev}} \leq Q_{n_m,t}^{agev} \leq \overline{S_{n_m,t}^{agev}} \ \forall n_m = 1, ..., LN, \forall t \tag{7}$$

$$\left(Q_{n_m,t}^{agev}\right)^2 + \left(P_{n_m,t}^{agev}\right)^2 \leq \left(\overline{S_{n_m,t}^{agev}}\right)^2 \ \forall n_m = 1, ..., LN, \forall t \tag{8}$$

where the aggregated EV load constraints are represented by (2)-(8), which include the aggregated EV energy consumption (2) obtained from travel information, the aggregated battery capacity (3), and the minimum SoC that is required at the end of the day (4). In the previous equations, τ_1 is the First Stage time step, $E_{agev_{n_m}}$ represents the aggregated EV energy at each MV node, $\overline{E_{agev_{n_m}}}$ is the maximum aggregated EV energy at each MV node, Bc_{ev} is the battery capacity of individual EVs, and $SoC_{agev_{n_m}}^{fin}$ and $SoC_{agev_{n_m}}^{ini}$ are the final and initial SoC values of the aggregated EV batteries. The aggregated power limits imposed by the rating of the chargers are considered in (5)-(8), where $\overline{S_{n_m,t}^{agev}}$ is the maximum aggregated EV apparent power, Cr_{ev} is the individual EV rating, and $Q_{n_m,t}^{agev}$ is the reactive power of the EV load. It is important to mention that EVs are modeled in this stage as aggregated loads that only absorb active power, as no discharge is considered in this paper, and can inject or absorb reactive power.

For LTCs, the constraints include the maximum and minimum tap positions, and the maximum number of operations per day, as follows:

$$\underline{tap_i} \leq tap_{i,t} \leq \overline{tap_i} \ \forall i, \forall t \tag{9}$$

$$\left|tap_{i,t} - tap_{i,t-1}\right| \leq Mop_{tap} \ \forall i, \forall t \tag{10}$$

Substation and feeder capacitor constraints are also considered, which are very similar to those of LTCs, as follows:

$$0 \leq cap_{j,t} \leq \overline{cap_j} \ \forall j, \forall t \tag{11}$$

$$\left|cap_{j,t} - cap_{j,t-1}\right| \leq Mop_{cap} \ \forall j, \forall t \tag{12}$$

These constraints include the limits for switching operations (11) and the maximum number of operations (12). The tap and switching positions of LTCs and capacitors are integer variable in this problem.

The First Stage also implements maximum and minimum voltage limits at MV nodes, current limits in distribution lines, and apparent power limit at MV nodes, as follows:

$$\underline{V_{n_m}} \leq V_{n_m,t} \leq \overline{V_{n_m}} \ \forall n_m, \forall t \tag{13}$$

$$0 \leq I_{l_m,t} \leq \overline{I_{l_m}} \ \forall l_m, \forall t \tag{14}$$

$$0 \leq |S|_{n_m,t} \leq \overline{S_{n_m,t}} \ \forall n_m, \forall t \tag{15}$$

Finally, unbalanced three-phase power flow equations relating P, Q, and voltages are also considered, as follows:

$$P_{n_m,p,t} = \sum_{k=1}^{N} \sum_{q=1}^{3} V_{n_m,p,t} V_{k,q,t} Y_{n_m,p,k,q} \cos(\theta_{n_m,p,k,q} + \delta_{n_m,p,t} - \delta_{k,q,t}) \ \forall n_m, \forall p, \forall t \tag{16}$$

$$Q_{n_m,p,t} = -\sum_{k=1}^{N} \sum_{q=1}^{3} V_{n_m,p,t} V_{k,q,t} Y_{n_m,p,k,q} \sin(\theta_{n_m,p,k,q} + \delta_{n_m,p,t} - \delta_{k,q,t}) \ \forall n_m, \forall p, \forall t \tag{17}$$

where $P_{n_m,p,t}$ and $Q_{n_m,p,t}$ are the active and reactive power injections at node n_m, phase p, at time t.

The initial step to solve the stochastic problem of the First Stage is to randomly define an initial time, initial SoC, and final time for each EV connected to the distribution feeder nodes. This random allocation is done using probability distribution functions (PDFs) derived from historical information of actual EVs, as in the present work; with this information, the maximum aggregated EV power and the required energy per node for the 24-hour period is determined. Then, the mixed integer nonlinear programming (MINLP) model described by equations (1)-(17) is solved using Matlabs Genetic Algorithm (GA) solver from the global optimization toolbox [25], and the OpenDSS package [26] to solve power flow constraints, from which the optimal transformer tap and capacitor schedules and the maximum daily peak for each aggregated EV realization can be obtained. The nonconvex MINLP nature of the First Stage problem does not guarantee the optimality of the obtained solution; however, GA approaches have demonstrated to be likely to find solutions that are close to the global optimum due to its search strategy [27]. Moreover, the OpenDSS package, which solves the power flow equations using a nodal admittance formulation, and a fixed point method to obtain feeder voltages and currents, is a well-known a robust power flow solution tool for distribution systems.

With the previous formulations, and using the genetic algorithm tool, the solution for a single realization of the EV load and forecast can be obtained in several minutes. Thus, employing a typical Montecarlo simulation (MCS) for obtaining good expected values and confidence intervals for this optimization model for the different load and EV forecast realizations would take several hours, which is not desirable in practice. To overcome this difficulty, the non-parametric bootstrapping method is used, as proposed in [23]. This method is an alternative to MCS and consists of obtaining a reduced number of samples of the population, much smaller than the number required in an MCS, and using random sampling

with replacement over these samples to obtain the statistics of a stochastic population. In this work, the aforementioned procedure to solve the First Stage optimization problem is repeated for 30 different EV load realizations, after which the non-parametric bootstrapping method is used to determine the best estimate of the maximum daily peak and the hourly tap and capacitor schedule considering EV uncertainties, as other loads are assumed here to be known, without loss of generality.

B. Second Stage

The tap and capacitor schedules and the maximum peak demand calculated in the First Stage are used as inputs in the Second Stage, which allocates the aggregated EV active and reactive power set points considering MV feeder constraints every 5 minutes. This allocation is done in such a way that EVs charge in a fast and fair manner, while providing support to the grid by injecting or absorbing reactive power. The following three objective functions are proposed:

1) The first is intended to allocate power in a fair manner and minimize voltage deviations:

$$\max \left(\alpha \sum_{n_m} \log \left(\frac{P^{agev}_{n_m,t}}{\overline{S^{agev}_{n_m,t}}} \right) - \beta \sum_{n_m} 100 \left(V_{n_m,t} - 1 \right)^2 \right) \ \forall t \tag{18}$$

where α and β are weight factors for the two components of the objective function. The fair allocation is done by maximizing the product of the ratios of EV active power at each node to the maximum EV charger capacity. In order to avoid scaling problems when many nodes are considered, the logarithm function is applied to the product, obtaining a summation function. The voltage deviation minimization is done by introducing the node voltage differences with respect to 1 p.u. in the maximization function. A coefficient is added for the purpose of objective function scaling.

2) In the second objective function, the aggregated EV active power is fairly allocated among the nodes, and the losses are minimized by introducing the differences between the sending and receiving end active power flows in all feeders lines in the maximization function:

$$\max \left(\alpha \sum_{n_m} \log \left(\frac{P^{agev}_{n_m,t}}{\overline{S^{agev}_{n_m,t}}} \right) - \beta \sum_{l_m} (P_{l_m,s,p,t} - P_{l_m,r,p,t})^2 \right) \ \forall t \tag{19}$$

where $P_{l_m,s,p,t}$ and $P_{l_m,r,p,t}$ represent the active power at sending and receiving ends of MV distribution lines.

3) The third objective function, which is referred here as voltage droop, maximizes the sum of the proportional fairness function and the aggregated EV droop constants, represented as $K^{agev}_{n_m,t}$:

$$\max \left(\alpha \sum_{n_m} \log \left(\frac{P^{agev}_{n_m,t}}{\overline{S^{agev}_{n_m,t}}} \right) + \beta \sum_{n_m} K^{agev}_{n_m,t} \right) \ \forall t \tag{20}$$

$$Q^{agev}_{n_m,t} = K^{agev}_{n_m,t} \left(V_{n_m,t} - 1 \right) \ \forall n_m, \forall t \tag{21}$$

$$0 \leq K_{n_m,t} \leq \frac{\overline{Q^{agev}_{n_m,t}} - \underline{Q^{agev}_{n_m,t}}}{1.04 - 0.96} \tag{22}$$

Equations (21) and (22) force the aggregated EV chargers to inject or absorb reactive power proportionally to the differences between the node voltage and 1 p.u. The voltage limits used to calculate the droop constants upper limit are chosen to be 1.04 and 0.96 p.u., which are within the tolerance band of $\pm 6\%$ for MV systems established in Canadian standards [28]. The formulation of this stage considers unbalanced voltage and currents in distribution lines, using ABCD parameters in a per-phase formulation, as follows:

$$\begin{bmatrix} \bar{V}_{s,p,t} \\ \bar{I}_{s,p,t} \end{bmatrix} = \begin{bmatrix} A & B \\ C & D \end{bmatrix} \begin{bmatrix} \bar{V}_{r,p,t} \\ \bar{I}_{r,p,t} \end{bmatrix} \ \forall l_m, \forall p, \forall t \tag{23}$$

Voltage and current expressions for loads correspond to a constant impedance model, as follows:

$$V_{L_m,p,t} = Z_{L_m,p,t} I_{L_m,p,t} \ \forall L_m, \forall p, \forall t \tag{24}$$

EV constraints, which include calculation of active and reactive powers for the aggregated EV loads, are represented as:

$$P^{agev}_{n_m,t} = Re \left\{ \sum_p V_{n_m,t} I^{agev^*}_{n_m,p,t} \right\} \ \forall n_m, \forall t \tag{25}$$

$$Q^{agev}_{n_m,t} = Im \left\{ \sum_p V_{n_m,t} I^{agev^*}_{n_m,p,t} \right\} \ \forall n_m, \forall t \tag{26}$$

In addition, the same first-stage constraints of active and reactive power limits imposed by the aggregated EV charger capacity (5)-(8) are included, and current balance in each node, which relates the currents in lines, transformers, capacitors, loads and aggregated EV loads are considered, as follows:

$$\sum_{l_m} I_{l_m,p,t} \left(\forall r_{n_m} \right) = \sum_{l_m} I_{l_m,p,t} \left(\forall s_{n_m} \right) + \sum_L I_{L_{n_m},p,t} + \sum_C I_{C_{n_m},p,t} + \sum_{n_m} I^{agev}_{n_m,p,t} \ \forall n_m, \forall p, \forall t \tag{27}$$

Finally, voltage limits for MV nodes (13) and current limits for distribution lines (14), and power limits for each node (15), which reflect the capacity of the low voltage transformer in each node are modeled, plus the maximum peak demand constraint, which is obtained from running the First Stage model, which is modeled as follows:

$$\sum_{n_m} \left(P^{bl}_{n_m,t} + P^{agev}_{n_m,t} \right) \leq P_{max} \ \forall t \tag{28}$$

The Second Stage formulation is non-linear, with no integer constraints, since the tap and capacitor positions are kept constant at the schedule found in the First Stage. This stage is coded in GAMS, and solved using the SNOPT solver [29].

C. Third Stage

Once the aggregated EV active and reactive powers are calculated, these signals are sent to the Third Stage, which allocates them among the EVs connected in the downstream LV system. In this stage, the allocation is done using the same fair approach as in the Second Stage. Hence, the objective function used for all cases, since the intention here is the disaggregation of active and reactive power set-points, is the following:

$$\max \sum_{ev=1}^{nev_{n_m,t}} \log\left(\frac{P_{ev,t}}{Cr_{ev}}\right) \forall t \tag{29}$$

The mathematical model of the Third Stage considers: voltages and currents in LV lines:

$$\begin{bmatrix}\bar{V}_{s,p,t}\\ \bar{I}_{s,p,t}\end{bmatrix} = \begin{bmatrix}A & B\\ C & D\end{bmatrix}\begin{bmatrix}\bar{V}_{r,p,t}\\ \bar{I}_{r,p,t}\end{bmatrix} \ \forall l_l, \forall p, \forall t \tag{30}$$

Voltage and current relationship for impedance load models:

$$V_{L_l,p,t} = Z_{L_l,p,t} I_{L_l,p,t} \ \forall L_l, \forall p, \forall t \tag{31}$$

EV active and reactive powers:

$$P_{ev,t} = Re\left\{\sum_p V^{ev}_{n_l,t} I^{ev^*}_{n_l,p,t}\right\} \ \forall ev = 1,..,nev_{n_m}, \forall t \tag{32}$$

$$Q_{ev,t} = Im\left\{\sum_p V^{ev}_{n_l,t} I^{ev^*}_{n_l,p,t}\right\} \ \forall ev = 1,..,nev_{n_m}, \forall t \tag{33}$$

The limits in active and reactive power for individual chargers:

$$0 \le P_{ev,t} \le Cr_{ev} \ \forall ev = 1,..,nev_{n_m}, \forall t \tag{34}$$

$$-Cr_{ev} \le Q_{ev,t} \le Cr_{ev} \ \forall ev = 1,..,nev_{n_m}, \forall t \tag{35}$$

And the following constraint to guarantee that the summation of individual EV active and reactive power consumptions is equal to the aggregated set-points:

$$\sum_{ev=1}^{nev_{n_m}} P_{ev,t} = P^{agev}_{n_m,t} \tag{36}$$

$$\sum_{ev=1}^{nev_{n_m}} Q_{ev,t} = Q^{agev}_{n_m,t} \tag{37}$$

The formulation of this stage also considers the current balance constraints:

$$\sum_{l_l} I_{l_l,p,t}\,(\forall r_{n_l}) = \sum_{l_l} I_{l_l,p,t}\,(\forall s_{n_l}) + \sum_{L} I_{L_{n_l,p,t}} + \sum_{n} I^{ev}_{n_l,p,t} \ \forall n_l, \forall p, \forall t \tag{38}$$

And limits in node voltages and distribution line currents:

$$\underline{V_{n_l}} \le V_{n_l,t} \le \overline{V_{n_l,t}} \ \forall n_l, \forall t \tag{39}$$

$$0 \le I_{l_l,p,t} \le \overline{|I|_{l_l,p,t}} \ \forall l_l, \forall p, \forall t \tag{40}$$

The Third Stage is also coded in GAMS, and solved using the SNOPT solver [29].

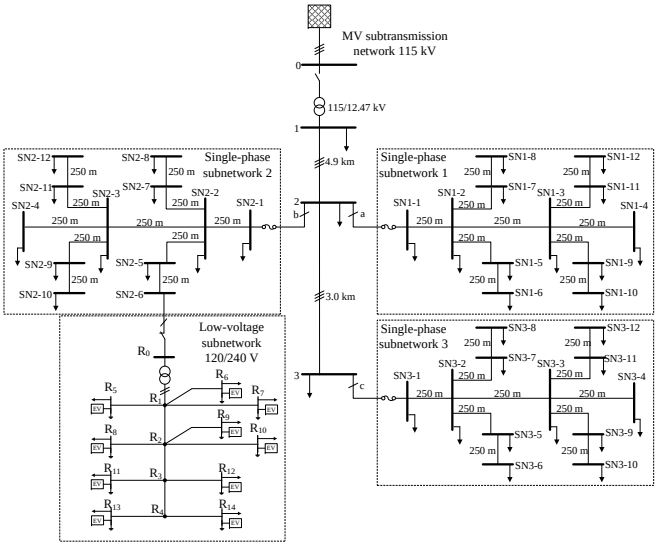

Fig. 2. MV and LV test systems.

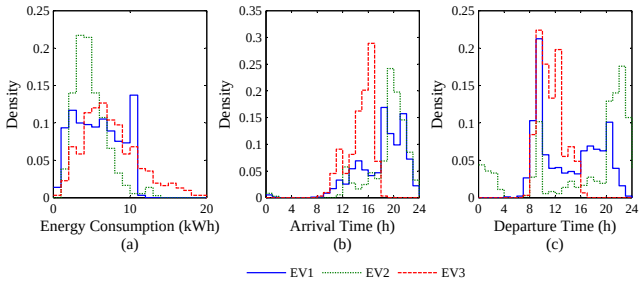

Fig. 3. (a) Energy consumption, (b) arrival time, and (c) departure time histograms for three EVs.

In every time step, after allocating the individual P and Q set points for each EV, the SoC is calculated using the following equation:

$$SoC_{ev,t} = SoC_{ev,t-1} + \frac{P_{ev,t}\ \tau_2}{Bc_{ev}} \ \forall t \tag{41}$$

where τ_2 is the Second Stage time step. If the SoC of an EV reaches 80%, P is not allocated for this EV in the next time steps, but Q is assumed to be available until the EV is no longer connected. This upper SoC limit is recommended by several EV manufacturers to extend battery life [30].

IV. Simulation Results and Analysis

A. Input Data, Test Systems, and Assumptions

The algorithm explained in the previous section was tested on a CIGRE's MV benchmark system [31]. The original benchmark system has a meshed feeder and a radial feeeder; in this study, however, only the more typical radial feeder shown in Fig. 2 was considered. This is a 12.47 kV feeder and has a length of 7.9 km. Three single-phase subfeeders, all having the same topology, are connected to the main feeder at different nodes and phases, and one subfeeder is modeled as an equivalent load at the first node.

In order to test the Third Stage of the algorithm, which operates at the LV level, the CIGRE's North American LV

benchmark system from [31] was employed. This LV feeder is composed of a 50 kVA, 12.47/240-120 V transformer, and 10 residential loads. To integrate the MV and LV test systems, the original loads at nodes SN1-6, SN1-7, SN1-9, SN2-6, SN2-7, SN2-9, SN3-6, SN3-7, and SN3-9 in Fig. 2 were replaced with the LV test system. Due to space constraints, only the LV system of node SN2-6 is represented in Fig. 2. The demand at each MV node that is not replaced by an LV system, follows the respective curves and peak values presented in [31] for the MV benchmark system; for those nodes modeled with the full LV system, the demand follows the individual household loads included in the report. Based on this, the peak base loads for the MV and LV systems are approximately 6000 kVA and 47 kVA, respectively, which corresponds to the original load of the benchmark system.

EV modeling is based on the actual data collected for three EVs operated in the region of Waterloo, Ontario, Canada, in a period of seventeen months[1]. The information used in this study was the consumed electricity between charging events, the arrival time, which determines the starting time for charging, and the departure time, which determines the maximum duration of the charging. Table I presents the general main data for the 3 EVs considered in the study, and Fig. 3 depict the corresponding histograms of energy consumption, and arrival and departure times. EV chargers for this study are rated at 3.3 kVA.

The original benchmark system considered in this study did not contain information about the number of households that represent the residential loads; hence, it is assumed here that for every 5 kVA of peak load, there is an EV charging in the system. Based on this assumption, Table II presents the number of EVs assumed to be connected to each node of the MV system. For the LV systems, it is further assumed that each household has an EV.

An existing heuristic EV charging control method was implemented, based on the calculation of sensitivities of node voltages to active and reactive power, and the use of a line-drop compensator (LC) to control the taps in the substation transformer. This heuristic technique is based on sensitivity factors that have been used for defining the location of DGs in distribution systems [32], and in the EV charging control problem [33]. The sensitivity factors are calculated by simulation, using dummy loads of 1 kW and 1 kVAR, which are placed at each one of the distribution system nodes to evaluate the change in voltages at all the nodes. The allocation of aggregated EV active and reactive power is done based on the following expressions:

$$P^{agev}_{n_m,t} = min\left(\gamma \frac{\Delta V_{k,t}}{max\left(\frac{\Delta V_{k,t}}{\Delta P_{n_m,t}}\right)}, \overline{P^{agev}_{n_m,t}}\right) \quad (42)$$

$$Q^{agev}_{n_m,t} = min\left(\gamma \frac{\Delta V_{k,t}}{max\left(\frac{\Delta V_{k,t}}{\Delta Q_{n_m,t}}\right)}, \overline{Q^{agev}_{n_m,t}}\right) \quad (43)$$

[1]The data was collected in the Drive4Data program, led by the Waterloo Institute for Sustainable Energy (WISE). More information is available at: https://wise.uwaterloo.ca/drive4data.

where γ represents a scaling factor, which in this case is equal to 0.1; $max\left(\frac{\Delta V_{k,t}}{\Delta P_{n_m,t}}\right)$ and $max\left(\frac{\Delta V_{k,t}}{\Delta Q_{n_m,t}}\right)$ represent the maximum sensitivity factors of all node voltages with respect to active and reactive power changes; and $\Delta V_{k,t}$ represents the desired voltage deviation at the node where the maximum sensitivity is recorded, and is calculated as follows:

$$\Delta V_{k,t} = \underline{V_{k,t}} - V^{bl}_{k,t} \quad (44)$$

where V^{bl}_{k} is the voltage at the kth node calculated at the base load conditions and no EVs.

The existing approach is also considered here for comparison purposes, and is referred to as business-as-usual (BAU). Thus, taps and capacitors are automatically controlled to keep the voltage at a certain point in the feeder fixed at a given value using an LC control, leaving EVs without control and thus allowing them to absorb their maximum P and Q capacities, i.e., $\overline{P^{agev}_{n_m,t}}$ and $\overline{Q^{agev}_{n_m,t}}$.

TABLE I
EV DATABASE SUMMARY

	EV model	Battery capacity (kWh)	Datalogging interval	# of charging events	Electricity consumed (kWh)
EV1	Chevy Volt '12	16	03/10/2014 - 08/14/2014	941	5078.05
EV2	Nissan Leaf '12	24	03/10/2014 - 08/14/2014	364	1589.78
EV3	Ford Focus EV '14	23	03/10/2014 - 08/14/2014	309	2143.39

TABLE II
NUMBER OF EVS PER MV NODE

MV node	# of EVs/node
SN1-5, SN1-8,SN1-11, SN1-12, SN2-5, SN2-8 SN2-11, SN2-12,SN3-5, SN3-8, SN3-11, SN3-12	2
SN1-1, SN1-2,SN1-3, SN1-4, SN1-10, SN2-1, SN2-2,SN2-3, SN2-4, SN2-10, SN3-1, SN3-2,SN3-3, SN3-4, SN3-10,	3
SN1-6, SN1-7,SN1-9, SN2-6, SN2-7, SN2-9, SN3-6,SN3-7, SN3-9	10
1	636

B. Simulation Results

First, the 3 EV models described in Table I were evenly assigned to the nodes of the test system, considering the number of EVs per node described in Table II, and 30 EV scenarios were created by randomly selecting one of the charging events available in the EV database. Each of these EV scenarios were then applied to the test system, and the First Stage optimization model was solved for each scenario, considering a full day and 1-hour time steps ($\tau_1 = 1$ hr). Then, 15000 bootstrapping samples were obtained from the 30 original samples of optimal maximum demand and optimal tap position for each hour. Figure 4 presents the maximum demand in the feeder during the entire day, before and after applying the nonparametric bootstrapping method. Figure 4(a) shows the original sample histogram, and Figure 4(b) presents the histogram of the mean maximum demand after applying

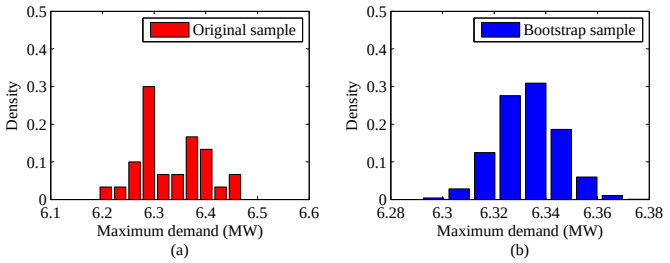

Fig. 4. Maximum demand histogram for (a) the original sample and (b) the bootstrap sample.

bootstrapping on the original sample. The shape of the latter histogram is close to a normal distribution, from which the expected value and the confidence interval of the system's maximum demand can be calculated.

Figure 5(a) plots the substation LTC tap position for the 24-hour period after applying bootstrapping to the original sample. The solid line represents the average tap position from the bootstrapping, and the error bars correspond to a confidence interval of 95.45%, or two standard deviations from the mean. The dotted blue line represents the final tap position after rounding the average values to integer values in order to apply it to the real system. The solution for each EV realization took in average 19 minutes, using Matlab 8.3.0.532 (R2014a) running in an Intel(R) Core(TM) i7-4770 CPU @3.40Ghz. Hence, the full solution for the First Stage took about 9.5 hours. Considering that this process is performed off-line the day before, these computational times allow for the practical application of this technique. However, these times can be significantly reduced if parallel computation approaches are used, since this stage can be readily parallelized as discussed in [23]. Figures 5(b) and 5(c) show the tap positions for the Heuristic and the BAU methods. In both cases, the LC was set to regulate the voltage at Node 3c in the main feeder to 0.99 p.u., with a band of 0.025 p.u; this voltage was chosen to obtain a total energy consumption similar to the optimization scenarios. Note that in these cases, the tap operation is more frequent compared to the First Stage results (22 and 23 number of operations in the Heuristic method and the BAU, respectively, and 7 in the proposed approach), so that the voltage is kept within the required range.

The Second Stage was tested by using one of the EV scenario from the First Stage, and the tap positions calculated in the First Stage were used as defined parameters for the Second Stage model. This stage was solved for five-minute periods (τ_2=5min) using the objective functions defined in (18)-(20); hence, 288 optimization runs were performed to complete a full day. Additionally, to test the sensitivity of the Second Stage results to the weights between the EV battery charging and the provision of reactive power, the following three sets of weights were used in functions (18)-(20): α=0.9 and β=0.1, α=0.5 and β=0.5, and α=0.1 and β=0.9 .

The voltages in the MV system are depicted in Fig. 6. Observe that in the optimization cases, voltages are similar because they use the same tap schedule, but they tend to be higher when losses are minimized. In the Heuristic and BAU

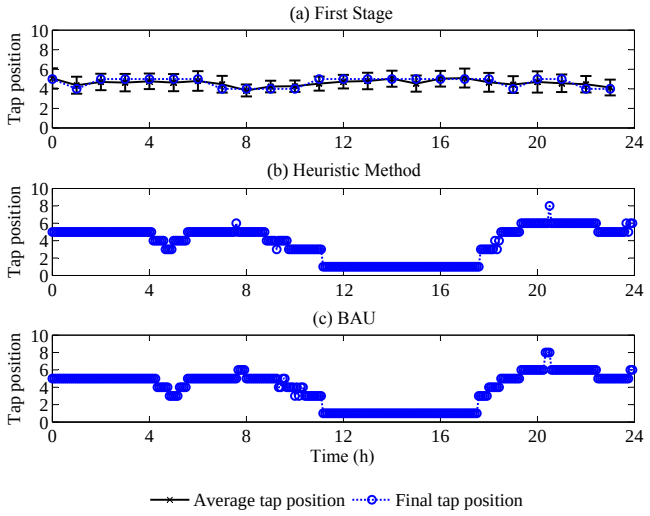

Fig. 5. Tap simulation results.

methods, the voltages are flatter compared to the other cases, since taps are operated constantly to keep the voltage within a given range. In all methods, the voltages are kept within the defined limits (0.96-1.04).

The resulting allocation of aggregated EV active and reactive powers for nodes SN1-7, SN2-10, and SN3-12 is presented in Fig. 7; these three nodes were selected since they are representative of different phases, demands and number of EVs. In Fig. 7, Case 1 represents the minimization of voltage deviations (18), Case 2 the minimization of losses (19), and Case 3 the voltage droop function (20). For the three optimization cases, only the results of the pair of weights that lead to a faster EV charging are presented. These plots show that aggregated EV active power is limited during times of peak demand due to LV transformer power limits. The sharp changes in P and Q in the plots are due to EVs arriving or leaving. Furthermore, reactive power is most of the time positive in Cases 1 and 3, because EV chargers try to lower the voltage, and negative in Case 2, since in this case the voltage is used to lower the currents and reduce losses. Each of these simulations took approximately 1.8 seconds, which demonstrates its practical feasibility for real-time applications. In the Heuristic method, P and Q are limited at times that do not necessarily coincide with the load peak in the corresponding LV system, thus leading to overload in the transformer. In the BAU method, this happens more often since vehicles are always allocated their maximum P and Q. This issue can be seen clearly in node SN3-12, around hour 6, where the optimization methods reduce the EV active power, but the Heuristic and BAU methods fully allocate the available capacity, overloading the corresponding MV/LV transformer.

Table III shows the summary of simulation results, including the total energy consumed by the EV fleet, the total losses in MV lines, the total energy consumed in the system, and the deviation of voltages with respect to 1 p.u. as per:

$$VD = \sqrt{\frac{1}{NT}\sum_{t=1}^{T}\sum_{k=1}^{N}(V_{k,t}-1)^2} \qquad (45)$$

TABLE III
ENERGY CONSUMPTION RESULTS

	EV Energy kWh	Energy Losses kWh	Total Energy kWh	VD
Case 1: Min. Voltage deviation (α=0.9 β=0.1)	5,449.71	180.71	109,790.72	1.46%
Case 1: Min. Voltage deviation (α=0.5 β=0.5)	5,237.27	177.38	109,583.29	1.44%
Case 1: Min. Voltage deviation (α=0.1 β=0.9)	5,717.01	169.27	110,077.03	1.40%
Case 2: Min. Losses (α=0.9 β=0.1)	5,908.95	175.66	110,256.31	1.65%
Case 2: Min. Losses (α=0.5 β=0.5)	6,026.83	169.5	110,400.31	1.60%
Case 2: Min. Losses (α=0.1 β=0.9)	5,952.69	168.2	110,327.14	1.59%
Case 3: Voltage Droop (α=0.9 β=0.1)	6,234.25	177.92	110,559.84	1.56%
Case 3: Voltage Droop (α=0.5 β=0.5)	6,091.64	176.38	110,419.69	1.55%
Case 3: Voltage Droop (α=0.1 β=0.9)	5,142.51	175.91	109,471.21	1.54%
Base case W/o Q control	6,097.62	182.53	110,403.48	1.65%
Heuristic method	5,989.62	192.29	110,540.44	1.76%
BAU	6,065.86	198.62	110,651.35	1.77%

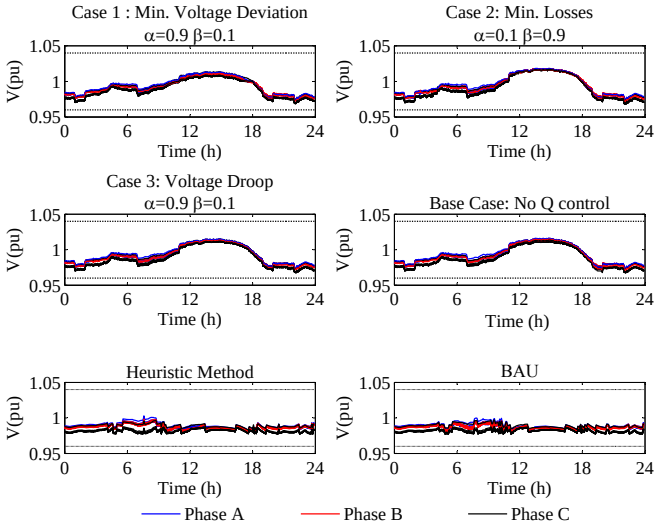

Fig. 6. Voltages in MV system

From these results, it can be seen that Case 1 scenarios present a lower EV energy with respect to the base case, with a difference in the range of 380 kWh to 860 kWh. Case 2 scenarios also exhibit a lower EV energy, but with smaller differences, ranging from 70 kWh to 188 kWh. Case 3 scenarios present the largest difference (955 kWh), and also the only scenario in which EV energy consumption is higher than the base case (136.63 kWh). The Heuristic method and BAU control method are very close to the base case, with differences of 108 kWh and 31 kWh, respectively. In terms of energy losses, Case 2 with α=0.1 and β=0.9 presents the largest reduction compared to the base case (7.85%); it is important to mention that these losses are calculated only for the MV lines and do not include the transformers and LV systems. The highest energy consumption is seen in the BAU scenario, while the lowest is seen in Case 3 with α=0.1 and β=0.9; the difference in consumption between these two scenarios is only 1180 kWh, and may be explained by the differences in losses, EV demand, and the modeling of loads as constant impedances. Finally, Case 1 scenarios present the lowest voltage deviations, ranging from 1.40% to 1.46%, while the voltage deviations in the Heuristic and the BAU methods are the highest, i.e. 1.76% and 1.77%, respectively. Note that in all these cases, the proposed holistic control approach reduces the losses and improve the voltage profiles with respect to previously proposed EV charging control approaches and the existing approach (BAU). However, this is accomplished at the expense of reducing the energy delivered to EVs, in a range of 0.1%-15%.

Figure 8 shows the individual allocation of active and reactive power set points of 3 different EVs in the LV network of node SN1-7. These set points are in agreement with the Second Stage results; note that the active power set point for each EV shows some differences with respect to the case with no Q control due to the provision of reactive power. Figure 9 presents voltage profiles at all buses in the LV system connected to Node SN1-7, under different control strategies; these are similar in shape to the voltages in the MV network shown in Fig. 6, and are within acceptable limits. Finally, Fig. 10 depicts the SoC curves for several vehicles during the hours the EV is connected to the charger. Observe that these two figures demonstrate that the provision of reactive power to the system has just a small impact on vehicle charging, which may result in the occasional case of the battery not reaching its maximum SoC in the available charging time. The Heuristic case, however, presents a higher delay in reaching the desired SoC since this node voltage in particular is more sensitive to load variations, which produces a lower allocation of EV power.

C. Discussion

Transformer taps and capacitors participate continuously in reactive power and voltage adjustment of distribution feeders under the control of LCs, with defined set points to keep the voltage at designated nodes within a given tolerance band; however, this approach may produce a high number of operations, leading to accelerated wear and tear of transformers and capacitors, which can be costly in terms of operation and maintenance. To reduce this adverse effect, transformer taps and capacitors in a distribution grid can be dispatched one day ahead within a volt/var control scheme, using load forecast information and constraining the number of transformer taps and capacitor operations per hour, as reported in, for example, [34] and [35]. This approach is built into the two-stage

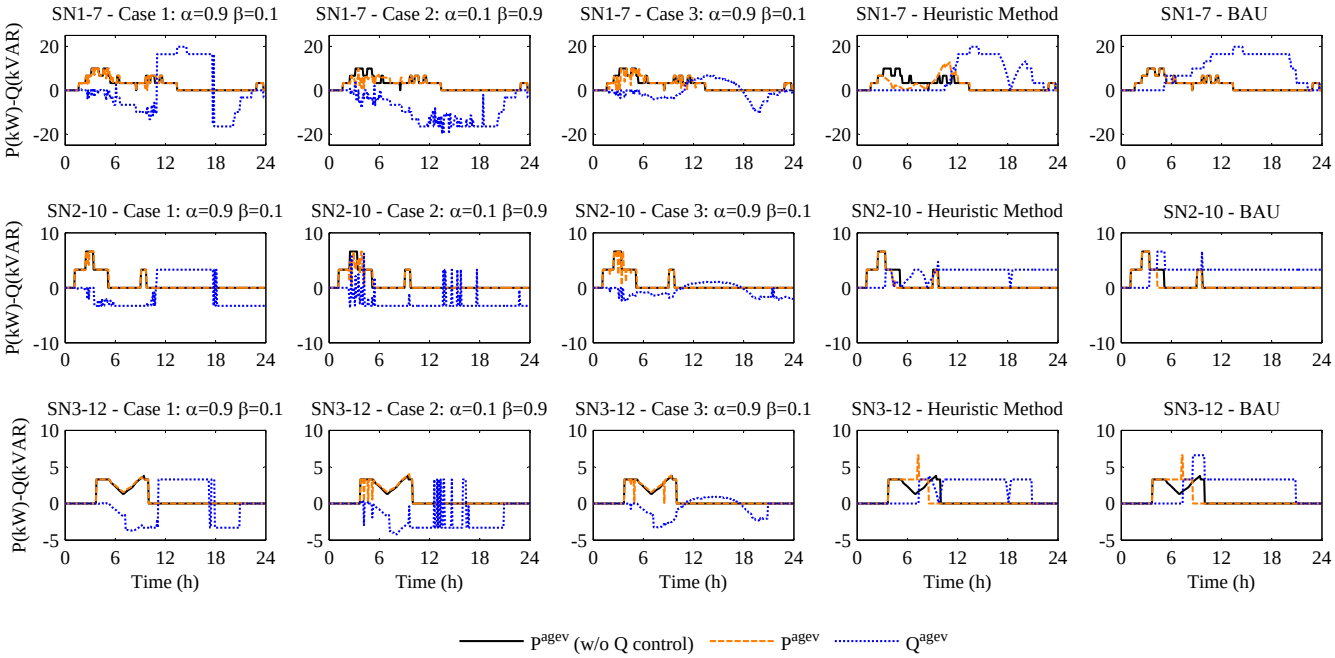

Fig. 7. Aggregated EV P and Q allocation at nodes SN1-7, SN2-10, SN3-12

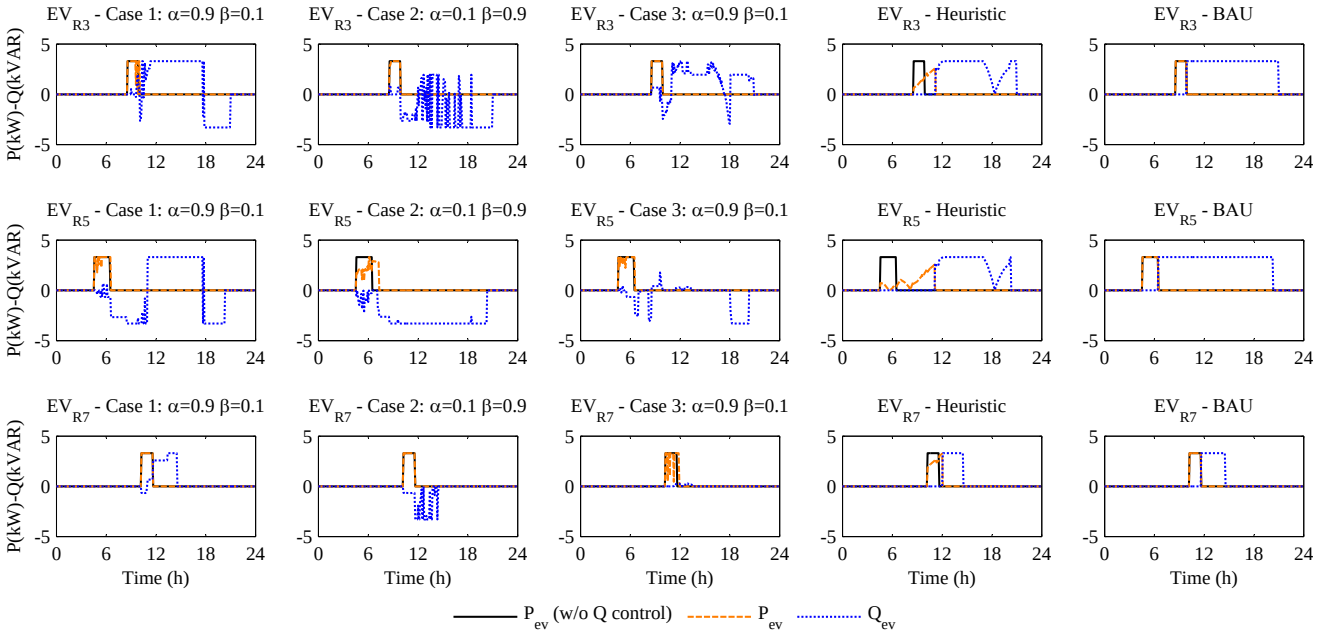

Fig. 8. Allocation of individual P and Q for EVs at SN1-7

technique proposed in [23] and [24], calculating the expected day-ahead optimal transformer tap and capacitor schedule based on a load peak minimization approach, including EVs as continuous reactive power sources. The day-ahead transformer tap and switched capacitor schedules are used in the Second and Third Stages, which make these mathematical models nonlinear programming problems (NLPs) that can be solved efficiently with commercial solvers, thus making them feasible for online applications.

So far, very few works have been published on the use of four-quadrant EV chargers to regulate voltage and reactive power in distribution feeders, considering both MV and LV levels. Hence, it is not possible to perform a full techno-economic comparison with respect to other similar works. Nevertheless, an estimation of costs of such a scheme can be obtained by considering that, based on [36], the cost of providing reactive power with a 3.3 kVA EV charger could be equal to 8.4 USD/kVAR per year (this value includes the incremental cost of upgrading a unidirectional ac/dc converter with a full bridge ac/dc converter, and the cost of additional losses),

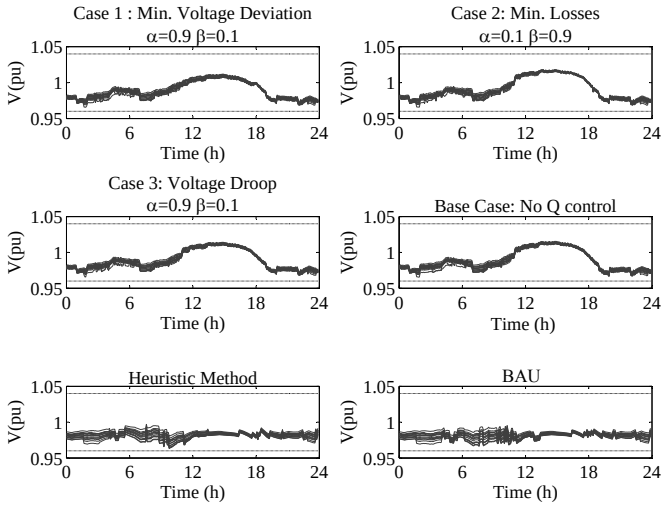

Fig. 9. Voltages at SN1-7

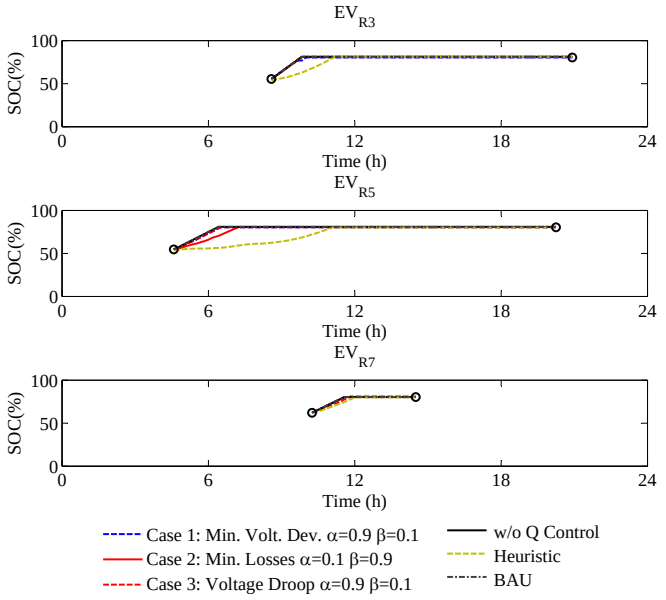

Fig. 10. SoC of EV batteries at SN1-7

compared to 2.8 USD/kVAR per year for a typical distribution capacitor bank; however, the volt/var control implemented by EV chargers would be distributed, continuous and accurate, in contrast with the case of distribution capacitor banks. Also, the implementation of the proposed holistic approach would reduce the number of transformer taps and switched capacitors, thus reducing wear and tear, and hence reducing maintenance costs [34]. Finally, the proposed volt/var control would reduce losses, thus reducing energy loss costs, as with any volt/var control approach in distribution systems [11].

V. Conclusions

This paper presented a three-stage algorithm for coordinating the operation of four-quadrant EV chargers and other volt/var control equipment in a distribution feeder. The outputs of each stage were used as inputs in the following stages to define the actual set points for EV chargers at the LV system. The First Stage included the uncertainties of EV users, and employed a non-parametric bootstrapping technique to calculate the confidence intervals of the optimal expected values for tap and switching capacitor positions and peak demand. The Second Stage allocated active and reactive powers for the EV aggregated demand at the MV nodes, using a proportional fairness approach and three different objectives for the volt/var function. The Third Stage distributed the active and reactive power set points calculated in the Second Stage among the individual EVs connected at the LV network. The algorithm was tested on a realistic CIGRE benchmark, comparing the results for the different objectives under study. The obtained results show that using the reactive power capacity of EV chargers improve the operation of distribution feeders by regulating the voltage and reducing losses, without having a significant effect on EV charging levels. Future work will study of simultaneous control of reactive power and battery discharging with four quadrant EV chargers in distribution feeders.

VI. Acknowledgment

The authors would like to thank Dr. Nafeesa Mehboob for her support in developing the proposed model.

References

[1] International Energy Agency, "Global EV outlook 2016," Tech. Rep., 2016. [Online]. Available: https://www.iea.org/publications/freepublications/publication/Global_EV_Outlook_2016.pdf

[2] J. A. P. Lopes, F. J. Soares, and P. M. R. Almeida, "Integration of electric vehicles in the electric power system," *Proc. IEEE*, vol. 99, no. 1, pp. 168–183, 2011.

[3] J. García-Villalobos, I. Zamora, J. San Martín, F. Asensio, and V. Aperribay, "Plug-in electric vehicles in electric distribution networks: A review of smart charging approaches," *Renewable and Sustainable Energy Reviews*, vol. 38, pp. 717–731, 2014.

[4] "Smart charging system for utilities, EVSE providers and fleets," Fleetcarma, 2016. [Online]. Available: http://www.fleetcarma.com/platform/electric-vehicles/smart-charging/

[5] M. Yilmaz and P. Krein, "Review of the impact of vehicle-to-grid technologies on distribution systems and utility interfaces," *IEEE Trans. Power Electron.*, vol. 28, no. 12, pp. 5673–5689, 2013.

[6] M. Kisacikoglu, B. Ozpineci, and L. Tolbert, "EV/PHEV bidirectional charger assessment for V2G reactive power operation," *IEEE Trans. Power Electron.*, vol. 28, no. 12, pp. 5717–5727, 2013.

[7] M. Kisacikoglu, M. Kesler, and L. Tolbert, "Single-phase on-board bidirectional PEV charger for V2G reactive power operation," *IEEE Trans. Smart Grid*, vol. 6, no. 2, pp. 767–775, March 2015.

[8] M. Restrepo, J. Morris, M. Kazerani, and C. Canizares, "Modeling and testing of a bidirectional smart charger for distribution system EV integration," *to appear in IEEE Trans. Smart Grid*, 2016.

[9] V. Monteiro, J. G. Pinto, and J. L. Afonso, "Operation modes for the electric vehicle in smart grids and smart homes: Present and proposed modes," *IEEE Trans. Veh. Technol.*, vol. 65, no. 3, pp. 1007–1020, 2016.

[10] M. Kesler, M. C. Kisacikoglu, and L. M. Tolbert, "Vehicle-to-grid reactive power operation using plug-in electric vehicle bidirectional offboard charger," *IEEE Trans. Ind. Electron.*, vol. 61, no. 12, pp. 6778–6784, 2014.

[11] T. Niknam, A. Ranjbar, and A. Shirani, "Impact of distributed generation on Volt/Var control in distribution networks," in *Proc. 2003 IEEE PowerTech*, vol. 3. IEEE, 2003, pp. 7–pp.

[12] B. A. Robbins, C. N. Hadjicostis, and A. D. Domínguez-García, "A two-stage distributed architecture for voltage control in power distribution systems," *IEEE Trans. Power Syst.*, vol. 28, no. 2, pp. 1470–1482, 2013.

[13] P. Jahangiri and D. C. Aliprantis, "Distributed Volt/VAr control by PV inverters," *IEEE Trans. Power Syst.*, vol. 28, no. 3, pp. 3429–3439, 2013.

[14] A. Kechroud, P. F. Ribeiro, and W. L. Kling, "Distributed generation support for voltage regulation: an adaptive approach," *Electric Power Systems Research*, vol. 107, pp. 213–220, 2014.

[15] T. Ding, S. Liu, W. Yuan, Z. Bie, and B. Zeng, "A two-stage robust reactive power optimization considering uncertain wind power integration in active distribution networks," *IEEE Trans. Sustainable Energy*, vol. 7, no. 1, pp. 301–311, 2016.
[16] T. Ding, R. Bo, H. Sun, F. Li, and Q. Guo, "A robust two-level coordinated static voltage security region for centrally integrated wind farms," *IEEE Trans. Smart Grid*, vol. 7, no. 1, pp. 460–470, 2016.
[17] Y. Mitsukuri, R. Hara, H. Kita, E. Kamiya, N. Hiraiwa, and E. Kogure, "Voltage regulation in distribution system utilizing electric vehicles and communication," in *Proc. 2012 IEEE PES T&D Conference and Exposition*. IEEE, 2012, pp. 1–6.
[18] H. Nafisi, S. M. M. Agah, H. A. Abyaneh, and M. Abedi, "Two-stage optimization method for energy loss minimization in microgrid based on smart power management scheme of PHEVs," *IEEE Trans. Smart Grid*, vol. 7, no. 3, pp. 1268–1276, 2016.
[19] B. Jiang and Y. Fei, "Decentralized scheduling of PEV on-street parking and charging for smart grid reactive power compensation," in *Proc. 2013 IEEE PES Innovative Smart Grid Technologies (ISGT)*. IEEE, 2013, pp. 1–6.
[20] M. N. Mojdehi, M. Fardad, and P. Ghosh, "Technical and economical evaluation of reactive power service from aggregated EVs," *Electric Power Systems Research*, vol. 133, pp. 132–141, 2016.
[21] M. Manbachi, H. Farhangi, A. Palizban, and S. Arzanpour, "A novel volt-var optimization engine for smart distribution networks utilizing vehicle to grid dispatch," *International Journal of Electrical Power & Energy Systems*, vol. 74, pp. 238–251, 2016.
[22] M. A. Azzouz, M. F. Shaaban, and E. F. El-Saadany, "Real-time optimal voltage regulation for distribution networks incorporating high penetration of PEVs," *IEEE Trans. Power Syst.*, vol. 30, no. 6, pp. 3234–3245, 2015.
[23] N. Mehboob, C. Canizares, and C. Rosenberg, "Day-ahead dispatch of distribution feeders considering temporal uncertainties of PEVs," in *Proc. 2015 IEEE PowerTech*. IEEE, 2015, pp. 1–6.
[24] N. Mehboob, "Smart charging of plug-in electric vehicles in distribution systems considering uncertainties," Ph.D. dissertation, University of Waterloo, 2016.
[25] "Global optimization toolbox documentation," The MathWorks, Inc., 2016. [Online]. Available: http://www.mathworks.com/help/gads/index.html
[26] "Simulation Tool - OpenDSS," Electric Power Research Institute, Inc. , 2011. [Online]. Available: http://smartgrid.epri.com/SimulationTool.aspx
[27] S. S. Rao, *Engineering optimization: theory and practice*. John Wiley & Sons, 2009.
[28] CSA, "CAN3-C23583: Preferred Voltage Levels for AC Systems 0 to 50000 V Electric Power Transmission and Distribution," 2015.
[29] P. E. Gill, W. Murray, M. A. Saunders, A. Drud, and E. Kalvelagen, "GAMS/SNOPT: an SQP algorithm for large-scale constrained optimization," *GAMS-The Solver Manuals*, 2000.
[30] J. Smart and S. Schey, "Battery electric vehicle driving and charging behavior observed early in the EV project," *SAE International Journal of Alternative Powertrains*, vol. 1, no. 2012-01-0199, pp. 27–33, 2012.
[31] K. Strunz *et al.*, "Benchmark systems for network integration of renewable and distributed energy resources," Tech. Rep. CIGRE Task Force C.04.02, 2013.
[32] V. Murthy and A. Kumar, "Comparison of optimal DG allocation methods in radial distribution systems based on sensitivity approaches," *International Journal of Electrical Power & Energy Systems*, vol. 53, pp. 450–467, 2013.
[33] A. O'Connell, D. Flynn, and A. Keane, "Rolling multi-period optimization to control electric vehicle charging in distribution networks," *IEEE Trans. Power Syst.*, vol. 29, no. 1, pp. 340–348, 2014.
[34] M. Liu, C. A. Cañizares, and W. Huang, "Reactive power and voltage control in distribution systems with limited switching operations," *IEEE Trans. Power Syst.*, vol. 24, no. 2, pp. 889–899, 2009.
[35] S. Paudyal, C. Cañizares, and K. Bhattacharya, "Optimal operation of distribution feeders in smart grids," *IEEE Trans. Ind. Electron.*, vol. 58, no. 10, pp. 4495–4503, 2011.
[36] M. C. Kisacikoglu, "Vehicle-to-Grid (V2G) reactive power operation analysis of the EV/PHEV bidirectional battery charger ," Ph.D. dissertation, University of Tennessee, Knoxville, 2013.

Mauricio Restrepo (S'13) received the electrical engineer degree and a specialization degree in transmission and distribution systems from Universidad Pontificia Bolivariana, Medellín, Colombia, in 2006 and 2010. He is currently working toward the Ph.D. degree in Electrical and Computer Engineering at the University of Waterloo, ON, Canada. His research interests include electric mobility, simulation and optimization of power systems.

Claudio A. Cañizares (S'85-M'91-SM'00-F'07) received the Diploma degree in electrical engineering from Escuela Politecnica Nacional, Quito, Ecuador, and the M.S. and Ph.D. degrees in electrical engineering from the University of Wisconsin-Madison, Madison, WI, USA, in 1984, 1988, and 1991, respectively. Dr. Claudio Cañizares is a Professor and the Hydro One Endowed Chair at the ECE Department of the University of Waterloo, where he has held different academic and leadership positions since 1993. His highly cited research activities focus on modeling, simulation, computation, stability, control, and optimization issues in power and energy systems in the context of competitive energy markets, smart grids, and microgrids. He is a Fellow of the IEEE, of the Royal Society of Canada, and of the Canadian Academy of Engineering, and is the recipient of the 2016 IEEE Canada Electric Power Medal and of other various awards and recognitions from IEEE-PES Technical Committees and Working Groups, in which he has held several leadership positions.

Mehrdad Kazerani (S'88-M'96-SM'02) received the B.Sc. degree from Shiraz University, Iran, the M.Eng. degree from Concordia University, Canada, and the Ph.D. degree from McGill University, Canada, in 1980, 1990, and 1995, respectively. From 1982 to 1987, he was with the Energy Ministry of Iran. He is currently a Professor at the Department of Electrical and Computer Engineering, University of Waterloo, Waterloo, ON, Canada. His research interests include power electronic circuits and systems design, power quality/active power filters, matrix converters, distributed power generation, utility interface of alternative energy sources, battery electric, hybrid electric and fuel cell vehicles, and FACTS. Dr. Kazerani is a Registered Professional Engineer in the province of Ontario.